



## Spatial distribution of Rare Earth Elements in a transnational watershed: The case of the Danube River

Pauline Louis<sup>a</sup>, Davide A.L. Vignati<sup>b</sup>, Steve Pontvianne<sup>a</sup>, Marie-Noëlle Pons<sup>a,c,\*</sup>

<sup>a</sup> Université de Lorraine, CNRS, LRGP, F-54000 Nancy, France

<sup>b</sup> Université de Lorraine, CNRS, LIEC, F-57000 Metz, France

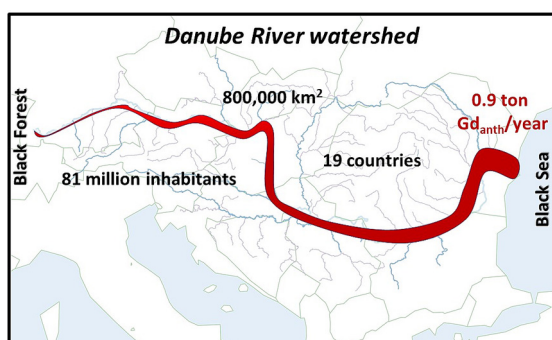
<sup>c</sup> LTSEZ-Zone Atelier du Bassin de la Moselle, LRGP, 54000 Nancy, France



### HIGHLIGHTS

- Rare Earth Elements patterns established along the Danube River for the first time.
- Gadolinium anomaly observed at short distances downstream the sources.
- More investigation needed for Ytterbium anomaly detected near the delta.

### GRAPHICAL ABSTRACT



### ARTICLE INFO

Editor: Damia Barcelo

### 1. Introduction

Rare Earth Elements (REEs), i.e. the fifteen lanthanides (from Lanthanum to Lutetium) to which Yttrium and Scandium are often associated, are increasingly present in our modern life: Y, La, Ce, Eu, Gd, and Tb in fluorescent lamps (Hobohm et al., 2016), Ce in batteries (Porvali et al., 2020), Nd, Pr and Dy in permanent magnets, La in catalysts (Kulaksız and Bau, 2011a), Ce in diesel fuel additives (Dale et al., 2017) are some examples. Anthropogenic uses of REE can both increase their concentrations above natural background levels and alter their natural distribution pattern by introducing anomalies in REE profiles. While the solid waste that may result from their use can be collected and potentially reprocessed (Hobohm et al., 2016; Yang et al., 2017; Porvali et al., 2020; Becci et al., 2021), the same is not true for REEs used in the medical field, in particular in contrast agents. These include Gd-based contrast agents (GBCAs), used in Magnetic

Resonance Imaging (MRI) examinations. GBCAs are eliminated through the urine and are therefore found in urban wastewater. These complexes are non-biodegradable and pass through wastewater treatment facilities to be released into aquatic environments. Since the first evidence (Bau and Dulski, 1996), the presence of Gd has been detected in aquatic ecosystems in many countries, even when they do not have MRI facilities. Table S1 provides data extracted from literature about Gd concentrations in non-saline surface waters around the world. It is difficult to calculate an average value as the data were obtained over 25 years in different hydrological conditions, in pristine waters as well as in highly urbanized areas. The highest value was measured (492 ng/L) in Postdam (Berlin/Brandenburg Metropolitan Area) by Kulaksız and Bau (2011b).

Although Gd is probably the most documented REE as a micropollutant of increasing concern, anthropogenic La has been detected in the Rhine River in Germany (Kulaksız and Bau, 2011a). In water samples (Kulaksız and Bau, 2013), samarium positive anomalies have been related to petrochemical industries, where Sm-based catalysts are used. Furthermore, the industrial activities related to the extraction and purification of REEs as

\* Corresponding author at: Université de Lorraine, CNRS, LRGP, F-54000 Nancy, France.  
E-mail address: [marie-noelle.pons@univ-lorraine.fr](mailto:marie-noelle.pons@univ-lorraine.fr) (M.-N. Pons).

well as REE-based products manufacturing can release REEs in aquatic ecosystems. According to Chen et al. (2021), contamination by REEs of the Qinhuai River in China might be related to electronic waste recycling and permanent magnet industries. In Dingnan County (China) heavy contamination of soil and water has been recorded close to a REEs mine (Liu et al., 2019). Mining activities not focusing directly to REEs can also be the source of contamination by these elements, as shown by Khan et al. (2016) in a former tin mining area. Runoff from agricultural fields where municipal sludge (Kaegi et al., 2021) and/or chemical fertilizers (Hu et al., 2004; Turra, 2018) have been applied can participate also to surface waters pollution by REEs. Urban runoff, contaminated by particulate pollution related to coal burning and transport activities, is also a contributor of La and Ce discharges in surface water (Shajib et al., 2020).

Once anthropogenic REEs are detected in surface water, there is a risk of transfer to drinking water. Bank filtration is used in many countries for drinking water production and its efficiency as a barrier against transfer of pharmaceutical residues has been questioned (Kondor et al., 2020). As early as 2009, Gd has been detected as a micropollutant in tap water in Berlin (Kulaksız and Bau, 2011b), with a rapid increase over a few years (Tepe et al., 2014). Bank filtration is not the only way to get anthropogenic Gd into tap water: karst aquifers can be easily contaminated as shown by Rabiet et al. (2009) in the Hérault watershed (France) and Boester and Rüde (2020) in Bavaria. Recently anthropogenic Gd has been reported in four tap waters in China, in the district of Guiyang (Han et al., 2021). If Gd-related health risks were thought to be minimal when GBCAs started to be used in the 1980s, more recent data indicate possible retention in different human organs such as kidney (Fraum et al., 2017), brain (Chazot et al., 2020) or bones (Veiga et al., 2020). Thomsen (2017) has suggested monitoring more closely Gd as risks associated with tap water are not well known. Accumulation of REE has been detected in many aquatic organisms (such as crabs (Lavezzo et al., 2020) and bivalves shells (Merschel and Bau, 2015; Le Goff et al., 2019; Mouchi et al., 2020; Valdés-Vilchis et al., 2021)) with the Gd anomaly linked to anthropogenic uses remaining detectable in bivalves (Pereto et al., 2020) and fish (Lortholarie et al., 2020). However, REEs seem to undergo biodilution along the food chain (Amyot et al., 2017; Santos et al., 2023) and the possible risks associated to their dietary uptake remain to be elucidated. Recently, Souza et al. (2021) discussed the evidence of high bioaccessibility of gadolinium-contrast agents after ingestion of Gd-contaminated tap water.

If anthropogenic REEs have been detected in different aquatic ecosystems, in particular in rivers, the number of samples collected is often limited to a couple as it can be seen in Table S1 (Supplementary Information section). It has to be recognized that sampling in watersheds of large rivers requires sophisticated logistics: Zhang et al. (1998) could only investigate the Yangtze River lower section (eight stations on about 1000 km of a 6300 km-long river) downstream of the city of Wuhan. Ma and Wang (2023) managed to sample 15 stations on tributaries of the complex Pearl River delta. In such cases, it is difficult to relate the REE concentration to the watershed characteristics and disentangle the actual contributions due to anthropogenic pressures from geological factors (Louis et al., 2020).

The fourth Joint Danube Survey (JDS4), which took place in summer 2019, was an extraordinary opportunity to monitor for the first time the REEs along the Danube River and in some of its tributaries. The Danube River watershed is the second largest in Europe with a surface of about 800,000 km<sup>2</sup> and is shared by nineteen countries, making it the most international river basin in the world, with a total population of 81 million inhabitants. Organized by the ICPDR (International Commission for the Protection of the Danube River) Monitoring and Assessment Expert Group, JDS4 made possible the sampling in twelve countries over a period of about one month (JDS4, 2021).

The purpose of the present study is to report for the first time the spatial distribution of REE concentrations in the Danube watershed and put this distribution in relation with those of other elements (alkaline earth metals, major ions (i.e., sulfates, chlorides and nitrates)), dissolved organic carbon

(DOC) concentration and typology and the population living in this transnational watershed.

## 2. Materials and methods

### 2.1. Sampling

The full list of all sample locations, with their codes, is given in the Supplementary Information section (Table S2 for the Danube River and Table S3 for its tributaries). Sampling upstream from Ulm took place July 3rd (between Neu Ulm and Donaueschingen) and July 4th 2019 (along the Breg River and the Brigach River between Donaueschingen and the river sources) (Fig. 1). Samples ( $n = 35$ ) were grabbed from bridges (except at the sources), 5 cm below the surface using a bailer made of high-density polyethylene (PEHD) (SDEC, Reignac-sur-Indre, France). Two tributaries were also sampled (Eisenbach River and Iller River) and two drinking water samples were collected in Donaueschingen and Ulm. The samples were transferred into clean 250 mL HDPE (High-Density PolyEthylene) bottles and kept in a coolbox in the dark until the arrival in the lab. They were then stored at 4 °C in the dark pending treatment within 24 h.

Sampling downstream from Neu Ulm took place in mid-July 2019, within the framework of the JDS4 (Fig. 2). The sampling team in each country had previously received clean 500 mL HDPE bottles. Fifty-one samples were grabbed along the Danube and some of its tributaries from the banks or from the middle of the river. Groundwater samples were also collected in wells recharged with Danube water through bank filtration in Austria, Slovakia, Hungary, Croatia, Serbia, Romania and Bulgaria (Fig. 2).

All samples were stored in a coolbox in the dark and transferred to the Environmental Institute (Kos, Slovakia) prior to their overnight shipment to France where they underwent pre-treatment within one day.

### 2.2. Analytical methods

#### 2.2.1. Sample filtration and ancillary parameters

Samples were filtered through regenerated cellulose syringe filters (Phenomenex®) with 0.45 µm nominal pore size. Only the filterable fraction, which consists of dissolved ions and colloids <0.45 µm, is considered in the present paper. Aliquots (50 mL for REEs, 10 mL for major elements) of the filterable fraction were acidified immediately after filtration with ultrapure HNO<sub>3</sub> (at 1 % v/v, acid class “Optima” for REEs and at 2 % v/v, acid class “Trace Metal” for major cations). Other sample aliquots (80 mL) were preserved at 4 °C without acidification for measurements of dissolved organic and inorganic carbon (DOC and DIC), total nitrogen (TN), major anions and characterization of the dissolved organic matter (DOM) by optical methods (section 2.3). DOC and DIC were measured with a Shimadzu TOC VCHS combined with a TNM-1 module for TN determination. Major anions (Cl<sup>-</sup>, SO<sub>4</sub><sup>2-</sup>, NO<sub>3</sub><sup>-</sup>) were determined by ion chromatography (Thermo Scientific Dionex iCS 3000) and major cations (Mg, Na, K, and Ca) by inductively coupled plasma atomic emission (ICP AES) (Thermo Scientific iCAP 6300 Duo).

#### 2.2.2. REEs analysis

REEs were determined using Inductively Coupled Plasma Mass Spectrometry (ICP-MS) (Thermo Scientific iCAPQ + prepFast) without preconcentration. Re and Rh at 50 ppb were used as online internal standards. The instrument was tuned for oxide and doubly charged ion formation, and interference corrections for oxide and hydroxide were applied when necessary. The analytical error was below 5 %. The quantification limit, calculated as 10 times the standard deviation of replicated blank measurements, was 1 ng/L for all REEs. The filtration blank results ( $n = 15$ ) were always below detection limits. SLRS-6 reference water was used to control the ICP-MS accuracy and reproducibility (Yeghicheyan et al., 2019) (Table S3).

The REEs concentrations were normalized by the Post Archean Australian Shale (PAAS) (McLennan, 1989; Rétif et al., 2023). The Ce and

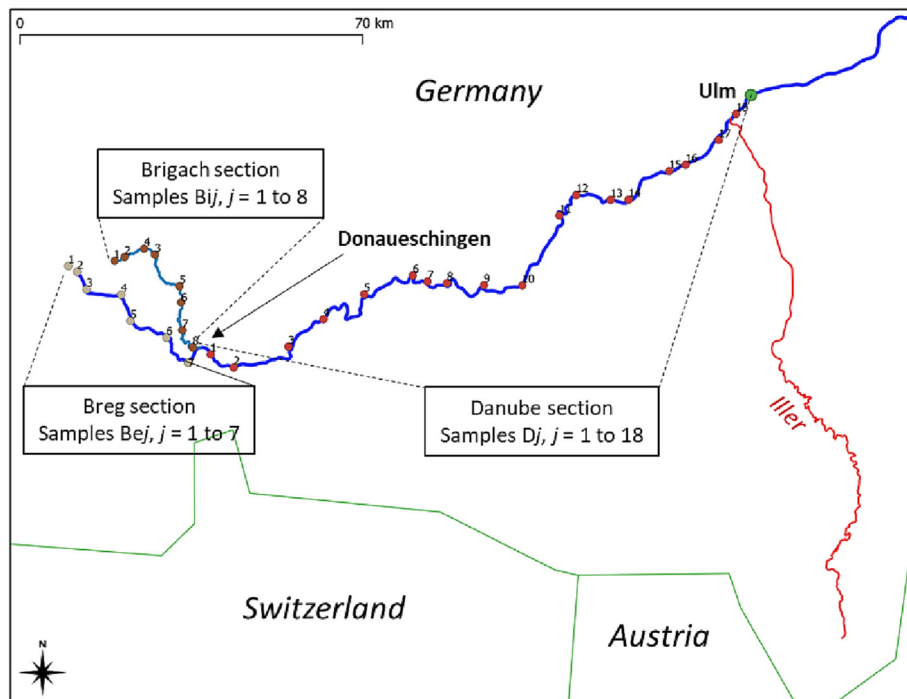


Fig. 1. Sampling sites along the Danube River between Ulm and Donaueschingen (samples D01 to D18), the Brigach River (samples Bi1 to Bi8) and the Breg River (Be1 to Be7).

Gd anomalies were calculated using Eqs. (1) and (2) (Hissler et al., 2015), respectively.

$$Ce/Ce^* = Ce_{PAAS} / (0.5 \times La_{PAAS} + 0.5 \times Pr_{PAAS}) \quad (1)$$

$$Gd/Gd^* = Gd_{PAAS} / (0.4 \times Nd_{PAAS} + 0.6 \times Dy_{PAAS}) \quad (2)$$

where X is the measured concentration in samples, X\* the calculated geogenic concentration, and X<sub>PAAS</sub> the concentration normalized by the

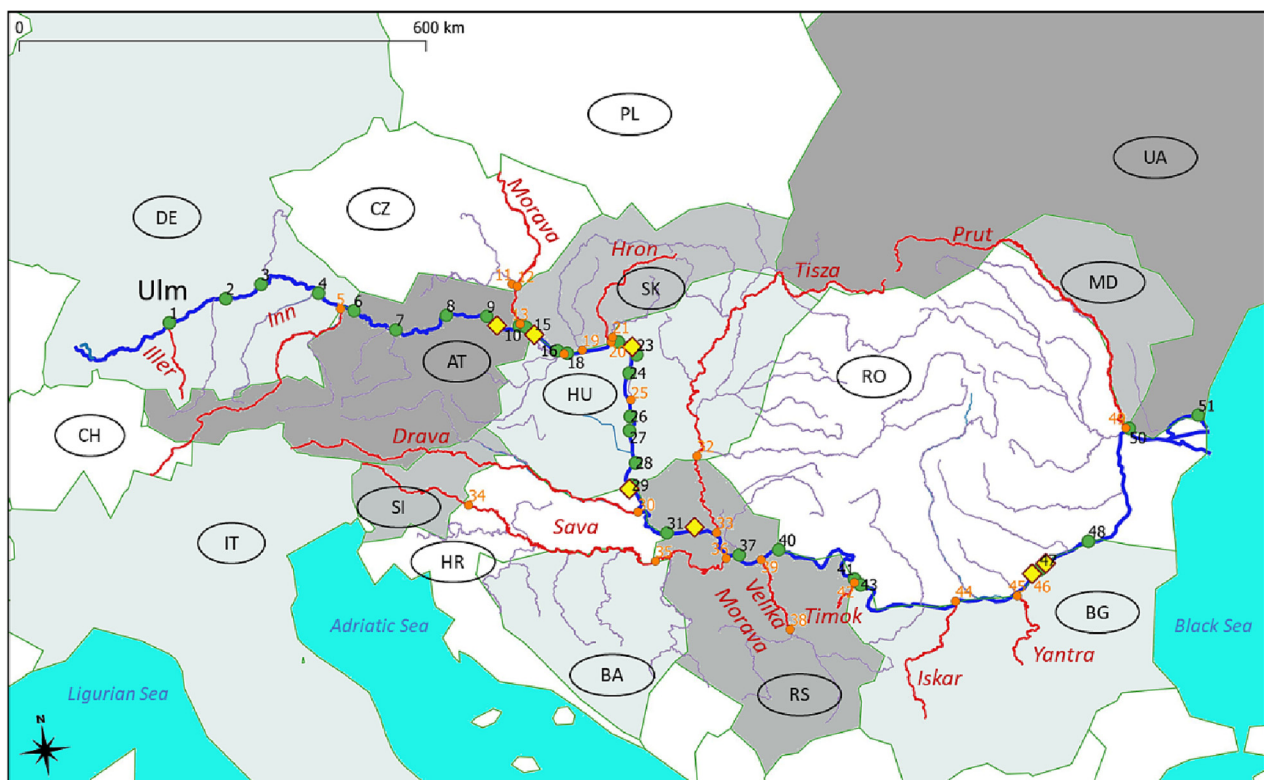


Fig. 2. Sampling sites along the Danube River between Ulm and the Black Sea (green dots) and some of its tributaries (orange dots) and groundwater samples (yellow diamonds).

PAAS. Finally the anthropogenic Gd concentration was deduced using Eq. (3):

$$Gd_{anth} = Gd - Gd^* \quad (3)$$

It should be noticed that the calculation method used in the present study for the Gd anomaly tends to maximize the value of the Gd anomaly compared with other calculation methods (Louis et al., 2020; Rétif et al., 2023).

### 2.3. Optical methods

Synchronous fluorescence spectra (SF50) were collected on a Hitachi F-2500 fluorimeter equipped with a Xenon lamp, by using FL Solution 2.0 software and a 1 cm × 1 cm 3.5 mL quartz cuvette. The gap between excitation and emission was set at 50 nm. The 50 nm deviation provides information on both fluorescence due to protein-like substances (excitation at around 280 nm) (Baker, 2002) and humic substances (humic acids and fulvic acids; excitation between 300 nm and 400 nm) (Coble, 1996). Since the absorbance of the sample may interfere with fluorescence, the absorbance at 254 nm was checked for each sample. UV-vis spectra (200–600 nm) were collected on a Shimadzu UV-2600 spectrophotometer, using a 1 cm × 1 cm quartz 3.5 mL cuvette. Ultra-pure water was used for blanks.

As  $A_{254}$  was  $<0.1 \text{ cm}^{-1}$  for 90 % of the samples, the absorbance was considered low enough to record fluorescence directly, without any correction for the inner-filter effect. The SF50 spectra were collected at the natural pH of the samples. The blank was performed with ultra-pure water. The fluorescence intensities were expressed in Raman units (R.u.).

To extract quantitative information out of the SF50 spectra, a decomposition procedure was applied (Assaad et al., 2015). In this approach, the synchronous fluorescence spectrum of a single fluorophore is represented by a Gauss function (Eq. (4)):

$$SF(\lambda) = F(b) \cdot \exp\left(-(\lambda - b)^2 / 2c^2\right) \quad (4)$$

where  $F(b)$  is the pseudo-concentration of the fluorophore,  $b$  (in nm) its characteristic excitation wavelength, i.e. the wavelength where the maximal fluorescence is recorded and  $c$  a parameter related to the width of the Gauss function. Each SF50 spectrum was decomposed into five Gauss functions (i.e., distinct fluorophores groups) by deconvolution. With a 50 nm gap the water Raman scatter interferes with the fluorescence of the fluorophore with a characteristic excitation wavelength of 355 nm and the contribution of water to this fluorophore is further corrected for.

### 2.4. Databases

Maps were constructed using Qgis 3.16 (<https://www.qgis.org>). Shape files for the Danube River and its main tributaries were extracted from the WISE database (<https://www.eea.europa.eu/data-and-maps/data/wise-large-rivers-and-large-lakes>). Brigach and Breg courses were obtained from the Baden-Württemberg Government (<https://rips-dienste.lubw.baden-wuerttemberg.de>).

The location and the capacity of the urban wastewater treatment plants along the Danube River and its (sub)tributaries were obtained from the dissemination platform of the Urban Waste Water Treatment Directive (UWWTD) (<https://uwwtd.eu/>) for the EU countries (2016 data) and from ICPDR for non-EU countries.

The 1:1,000,000 geological (GK1000) data of Germany were downloaded from the database of the federal Institute for Geosciences and Natural Resources (<https://www.bgr.bund.de>).

Ancillary data for DOC and nitrates were compared to the 2017 water quality data provided by ICPDR through the TransNational Monitoring Network (TNMN) scheme ([https://www.icpdr.org/main/sites/default/files/nodes/documents/tnmn2017\\_annex\\_1.xls](https://www.icpdr.org/main/sites/default/files/nodes/documents/tnmn2017_annex_1.xls)). Flow rates in some specific stations were measured during the JDS4 and retrieved from the JDS4 database (<https://data.danubsurvey.org/jds4/>).

The Eurostat database provided the data about the number of MRI examinations in Europe (<https://data.europa.eu>). Complementary data for non-EU countries were extracted from the OECD Health Database (<https://www.oecd.org/els/health-systems/health-data.htm>).

The distances are established from the mouth at the Black Sea for the Danube River and from the confluence with the Danube River for its tributaries. The Danube River is divided into three main parts: the Upper Danube River refers to the river course between the sources and rkm 1789.5 (Klížská Nemá, Slovakia); the Middle Danube River to the river course between rkm 1789.5 and rkm 943 (Turnu Severin, Romania); the Lower Danube River to the river course between rkm 943 and the Black Sea ([https://www.icpdr.org/flowpaper/viewer/default/files/roof\\_report\\_2004\\_annexes.pdf](https://www.icpdr.org/flowpaper/viewer/default/files/roof_report_2004_annexes.pdf)).

## 3. Results and discussion

### 3.1. Physical-chemical parameters

This section summarizes the main characteristics of the surface water of the Danube, and particularly those related to dissolved organic matter (DOM) and nitrates which can provide information on the global anthropogenic pressure on the river basin.

In their upper parts, the Brigach River and the Breg River are flowing on silica-rich rocks (granite, sandstone). Their concentrations in alkaline minerals (calcium, magnesium, potassium and sodium) increase gradually moving downstream where they are leaching Triassic and Jurassic rocks (i.e. limestone, marlstone) (Fig. S1 and Table S5). At Ulm, the Danube River meets the Iller River, its first large tributary (Fig. 3). This alpine river average flowrate at the confluence is larger than the Danube River average flowrate (70 m<sup>3</sup>/s versus 53 m<sup>3</sup>/s), which causes a strong dilution. This dilution (Fig. S2) is further accentuated at the junction with the Inn River, a large alpine tributary of low mineral content (Table S5) whose discharge flowrate is similar to that of the Danube at their junction ( $\approx 2200$  rkm). The Inn River has its maximal flowrate in summer due to the snow melting in the Alpine upper part of its watershed (Fig. S3). Its dilution effect is seen on the mineral content of the Danube waters (Fig. S2). Downstream Passau, the calcium, magnesium and potassium concentrations are stable until the Danube reaches the Black Sea. The sodium concentration increases, which can be seen as a result of the discharge, in the aquatic environment, of urban wastewater containing detergent residues.

DOC is higher in the samples collected upstream Ulm, in particular in the waters of the Brigach River and of the Danube River, than downstream Ulm (average of 3.1 mg/L and 2.0 mg/L respectively) (Fig. 4). The Inn River carries very little DOC (0.5 mg/L in Passau-Ingling) (Table S4). DOC does not vary much in the middle section of the Danube River (average of 1.7 mg/L). Large inflows from the tributaries (up to 7.5 mg/L for Morava River) are quickly diluted: the Morava River discharge rate is only 6 % of the Danube River at their junction. In the Lower Danube, DOC increases (average 2.8 mg/L), which seems to be controlled by inflows from tributaries with less dilution effects than upstream. This increase in DOC in the Lower Danube was also highlighted during the JDS3 campaign (Joint Danube Survey 3, 2015).

Synchronous fluorescence spectra and their deconvolution provide further insight into the nature of DOM (Fig. 5). Protein-type fluorophores are linked to biological reactions in water but also to the runoff of biological substances from the watershed and the discharge of raw sewage or insufficiently treated urban wastewater. Their fluorescence is largely due to the presence of the indole group which is present in tryptophan (an essential amino acid for humans, which is produced only by microorganisms and plants), in auxins (plant hormones) and in acids bound to urine (such as, for example, 5-hydroxy-indolylacetic acid, a metabolite of serotonin). Other fluorescent substances that can be found in the same spectral region as tryptophan in the SF50 spectra are threonine ( $\lambda_{exc} \approx 280$  nm), another essential amino acid for humans, and tyrosine ( $\lambda_{exc} \approx 270$  nm), also an amino acid.

In the Danube watershed, the total pseudo-concentrations of fluorophores vary from 0.042 to 0.235 Raman units. These pseudo-

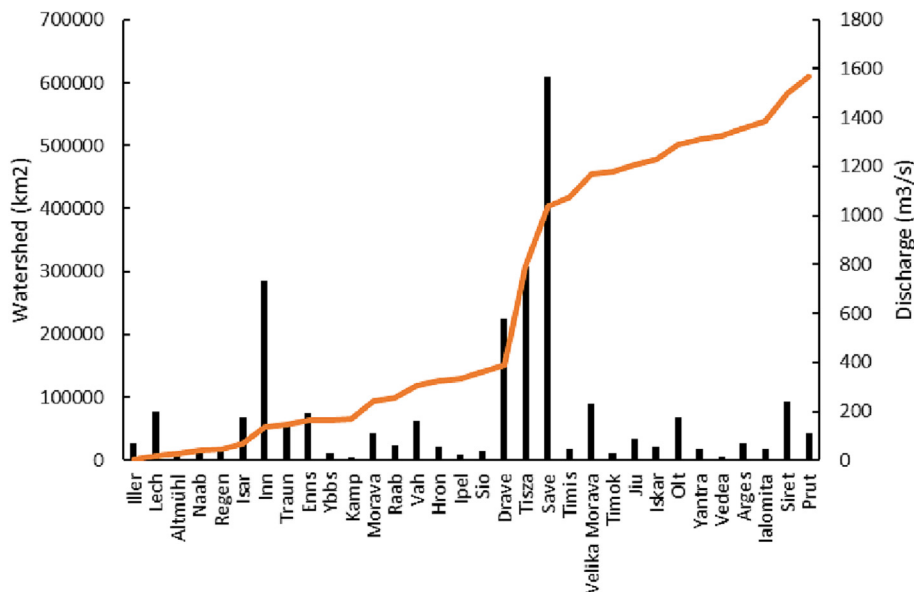


Fig. 3. Danube River watershed area (in orange) as a function of the received tributaries (average annual discharge in black).

concentrations are globally higher for the samples from the Brigach River and the Upper Danube River (0.065 to 0.235 Raman units). They decrease in the Median Basin (0.042 to 0.105 Raman units) before increasing after the confluence with the Timok (SW42-Tim) in the Lower Basin and the Delta (0.074 to 0.141 Raman units). The Eisenbach River, the Iller River and the Inn River carry little fluorescence. Other tributaries such as the Morava River, the Hron River, the Ipel River, the Tisza River and the Sava River bring a high quantity of fluorescent dissolved organic matter in the Upper and Middle sections of the Danube River Basin (0.114 to 0.208 Raman units). However, these contributions seem to disappear rapidly under the effects of dilution with the Danube River waters, as observed for the DOC values. In the Lower section of the Danube River basin and in its delta, the contribution of other tributaries (Iskar River, Yantra River, Russenski Lom River and Prut River) is also significant (0.103 to 0.211 Raman units) and seems less affected by dilution effects, as the fluorescence of the River Danube waters is higher downstream.

In the Upper Basin, the fluorophores of the protein type (F (280) and F (310)) represent 47 to 82 % of the total fluorescence, and the fluorophores of the humic-fulvic type (F (330), F (355), F (370)) 18 to 53 %. In the Middle Basin, protein-type fluorophores represent 39 to 70 % of the total fluorescence, and humic-fulvic-type fluorophores 30 to 61 %. Finally, in the Lower Basin and in the delta, protein-type fluorophores represent 40 to

61 % of the total fluorescence, and humic-fulvic-type fluorophores 39 to 60 %. Downstream Ulm, there is no clear prevalence of protein-like or humic-fulvic-like DOM in the Danube River watershed, except for some tributaries (such as Morava River, Hron River, Ipel River, Prut River). The humic-fulvic-like DOM is partly of allochthonous origin (terrestrial origin resulting from the degradation of plants) of the DOM, due to soil leaching. An anthropogenic origin can also be assumed due to discharge of non-biodegradable pollution originating from wastewater treatments plants effluents. The DOM of the upstream part shows, by contrast, a rather autochthonous origin, resulting from the biological activity of algae or bacteria (the Danube being quite shallow upstream of Ulm, aquatic plants and algae development could be favored by facilitated photosynthesis), or treated wastewater discharged from WWTPs. The high population density, such as the one observed in Germany ( $\approx 230 \text{ inh/km}^2$ ) combined with relatively small flowrates, especially in summer, induces low dilution rates of treated wastewater in the receiving bodies. The average yearly flowrates of the Brigach River and the Breg River at Donaueschingen are  $3.3 \text{ m}^3/\text{s}$  and  $5 \text{ m}^3/\text{s}$ , respectively (<https://www.hvz.baden-wuerttemberg.de/>).

Nitrates can be introduced into aquatic systems via atmospheric emissions, fertilizer runoff and effluents from wastewater treatment plants. Nitrates are higher in the waters of the Brigach River and in the samples from the Danube River between Donaueschingen and Ulm than in the

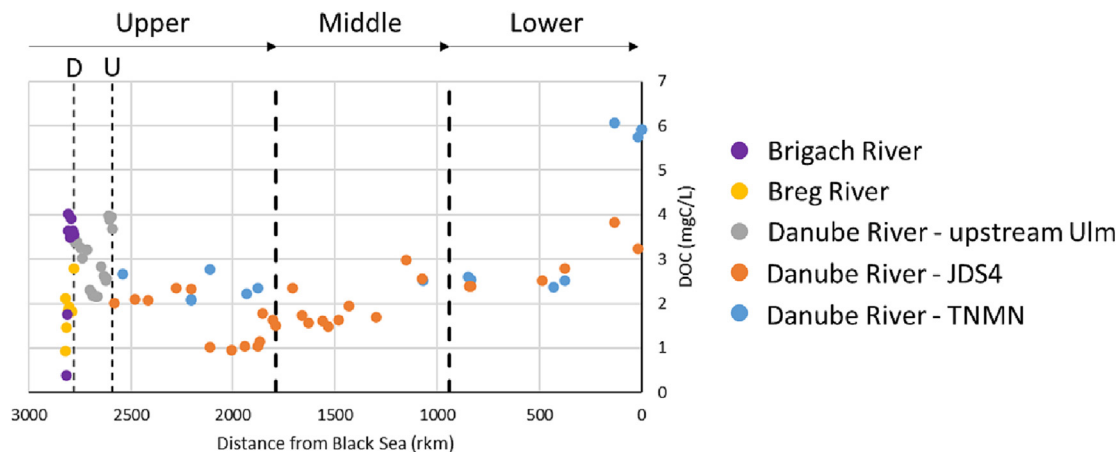


Fig. 4. Dissolved organic carbon (DOC) along the Danube River. D = Donaueschingen, U = Ulm. JDS4: Joint Danube survey 4 (present study), TNMN, Trans-National Monitoring Network (2017).

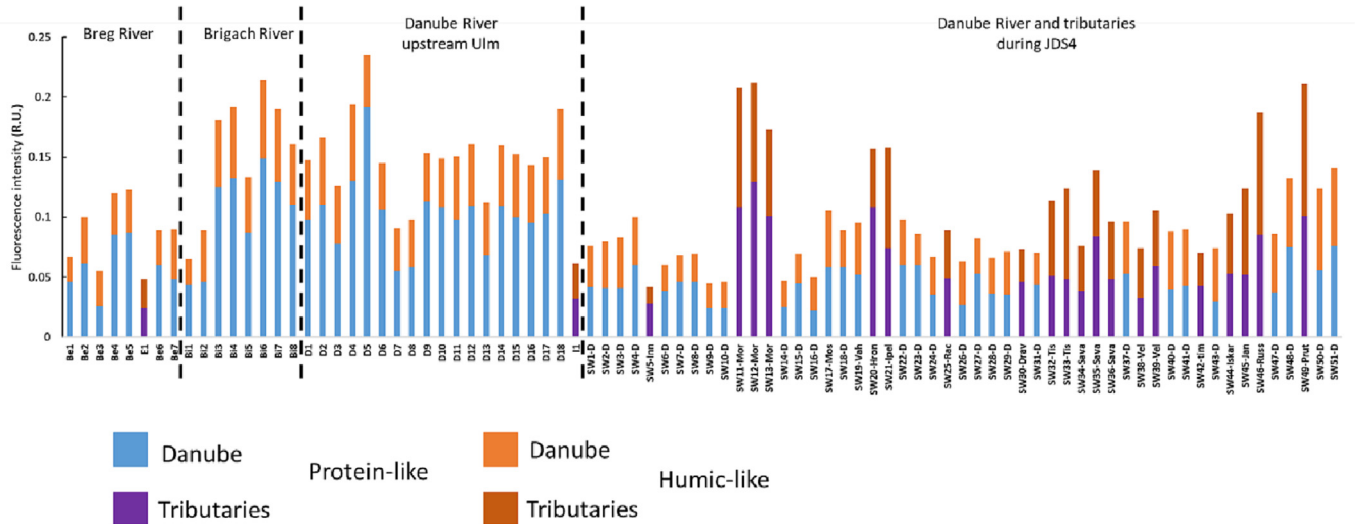


Fig. 5. Protein-like and humic-like fluorescence in the Danube River watershed in July 2019.

samples from the JDS4 (Fig. 6). Among the tributaries of the Danube, the Russenski Lom (Bulgaria) has the highest concentration (29.8 mgNO<sub>3</sub>/L), but its contribution disappears in the waters of the Danube with the effects of dilution. During the 2013 JDS3 campaign, Russenski Lom already showed the highest nitrate concentration (5.2 mg/L N-NO<sub>3</sub> or 23 mgNO<sub>3</sub>/L) (JDS3 report, 2015), and a decrease in the nitrate concentration was observed from upstream (Ulm, Germany) to downstream (delta) for the Danube River waters (from 14 to 3.9 mgNO<sub>3</sub>/L). The nitrate concentration is practically stable between rkm 2250 (junction with the Inn River (running down from the Aps mountains)) and the delta. This means that the nitrate flux becomes larger as the Danube River flows toward the Black Sea.

In conclusion, once the Danube River meets its first large tributaries (Iller River in Ulm and Inn River in Passau) the potential anthropogenic pressure exerted by the watershed is rather diffuse and no hot spot can be detected, either for nitrogen species or dissolved organic carbon. In particular, the dissolved organic carbon is slowly increasing, which can be explained by the increase of the served population from upstream to downstream.

### 3.2. REE spectra and anomalies

Fig. 7 shows the REE normalized patterns for the Breg River and the Brigach River. The most upstream section of both rivers present patterns with flat sections between Dy and Lu (Heavy REE or HREE). These patterns are similar to those observed by Louis et al. (2020) for headwaters in the Vosges mountains, running on a similar geology (granite, sandstone). A

negative Ce anomaly, induced by the redox characteristics of cerium, can be noticed for both rivers (Elderfield et al., 1990). Indeed, Ce can have two oxidation states (Ce<sup>3+</sup> and Ce<sup>4+</sup>) in the typical conditions of temperature and pressure of surface water and Ce<sup>4+</sup> is likely to combine with oxygen to form cerianite. As cerianite is very insoluble, its formation leads to Ce negative anomaly in water (Seto and Akagi, 2008). Along the Danube River, all samples but two exhibit a negative Ce anomaly (Fig. S5) with an average value (± one standard deviation) of 0.66 ± 0.14 between Donaueschingen and Ulm and a slight trend downstream of Ulm (coefficient of determination R<sup>2</sup> = 0.14).

The La/Lu ratio varies between 0.05 and 0.35 in the Breg and Brigach river and tends to increase along their courses indicating a gradual depletion in LREE with respect to HREE (Fig. S6). No clear trend is observed between Donaueschingen and Ulm for the La/Lu ratio because of the variable geology (marlstone, limestone) of the Danube basin in this section combined with possible anthropogenic influences (see below). The sampling is not sufficiently dense in this section to go deeper in the discussion. Between Passau (junction with the Inn River) and the Black Sea, the La/Lu ratio decreases slowly (R<sup>2</sup> = 0.18), revealing an increasing fractionation of the REE pattern. The observed decrease indicates increasing inputs from urban and industrial wastewater treatment plants along the Danube River, in agreement with the increase in sodium concentration. Indeed, highly fractionated REE patterns with LREE depletion and marked Gd anomalies are typical of wastewaters (Martin et al., 2021). The explored tributaries present La/Lu ratios lower than those observed on the Danube

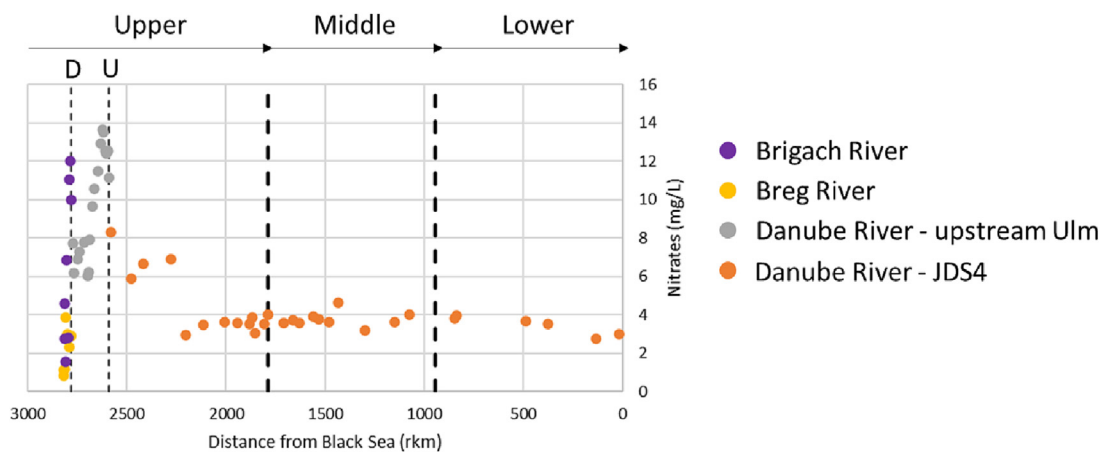


Fig. 6. Nitrates along the Danube River. D = Donaueschingen, U = Ulm.

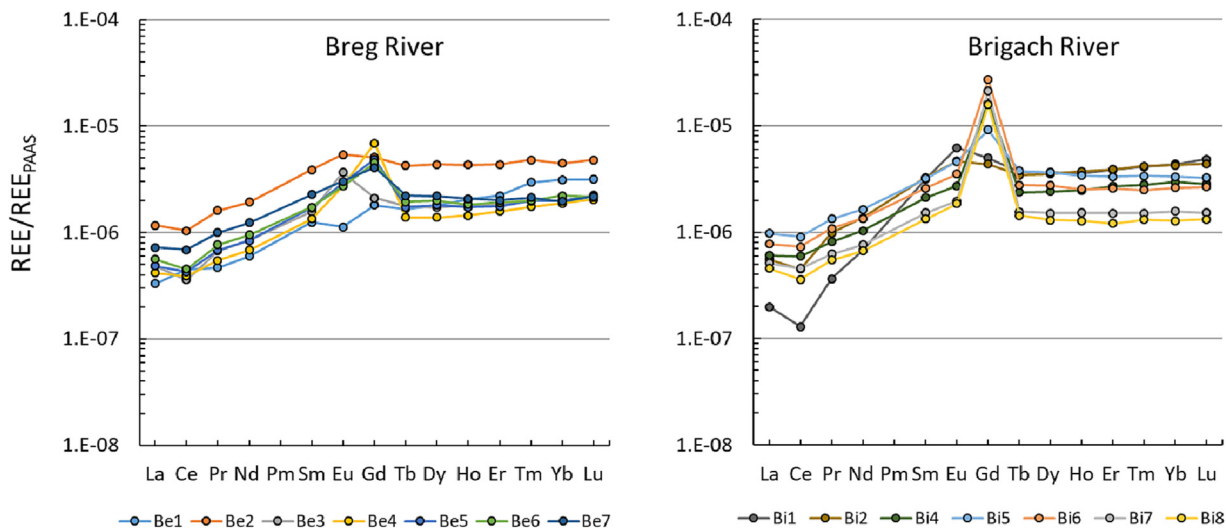


Fig. 7. REE patterns, normalized with respect to PAAS, along the Breg River and the Brigach River.

River, suggesting a more marked impact of wastewater discharges in these water courses.

Gd anomalies are detected on the Breg River at the Vörenbach station (Be4) and on the Brigach River at the Sankt Georgen station (Bi3), about 10 km downstream their sources. All the samples collected between Donaueschingen and Ulm present a strong Gd anomaly (between 2.8 at station D2 and 10.9 at station D12).

Further downstream, the Gd positive anomaly is detectable in all the samples (Gd/Gd\* value from 1.85 to 37.41), except in sample SW-46 (Russenski Lom, tributary in Bulgaria with Gd/Gd\* = 1.18) (Figs. 8 and S4). To define a Gd anomaly as an anthropogenic anomaly, the threshold value of Gd/Gd\* is usually set to 1.5 (Bau et al., 2006). In the case of the Danube River and its tributaries, the visible Gd anomalies are always above this threshold value: that allows the calculation of Gd<sub>anth</sub> concentrations. For the Danube River itself, the most important Gd/Gd\* value is for

the sample JDS4-4 (Gd/Gd\*: 25.9). This sampling station is located in Germany, just downstream a WWTP effluent discharge.

Only one other study has reported a positive Gd anomaly in Danube River. This is by Kulaksız and Bau (2011b), who analysed a sample grabbed in Austria. Using their data with the Nd and Dy calculation method, the Gd/Gd\* anomaly is 2.8 and the Gd<sub>anth</sub> concentration is estimated at 47 ng/L. The JDS4 samples from SW6-D to SW10-D were collected in Austria. Their Gd/Gd\* values are higher (from 10.8 to 18.1) for a lower calculated Gd<sub>anth</sub> concentration (from 8.3 to 9.5 ng Gd<sub>anth</sub>/L), which can be explained by the fact that the overall REE amounts for JDS4 are lower than for the study by Kulaksız and Bau (2011b). However, as the exact location and sampling period of the Kulaksız and Bau (2011b) study are not known and it is difficult to establish a meaningful comparison.

Based on the values of Gd/Gd\* and the corresponding calculated Gd<sub>anth</sub> concentrations two groups can be identified clearly along the Danube River

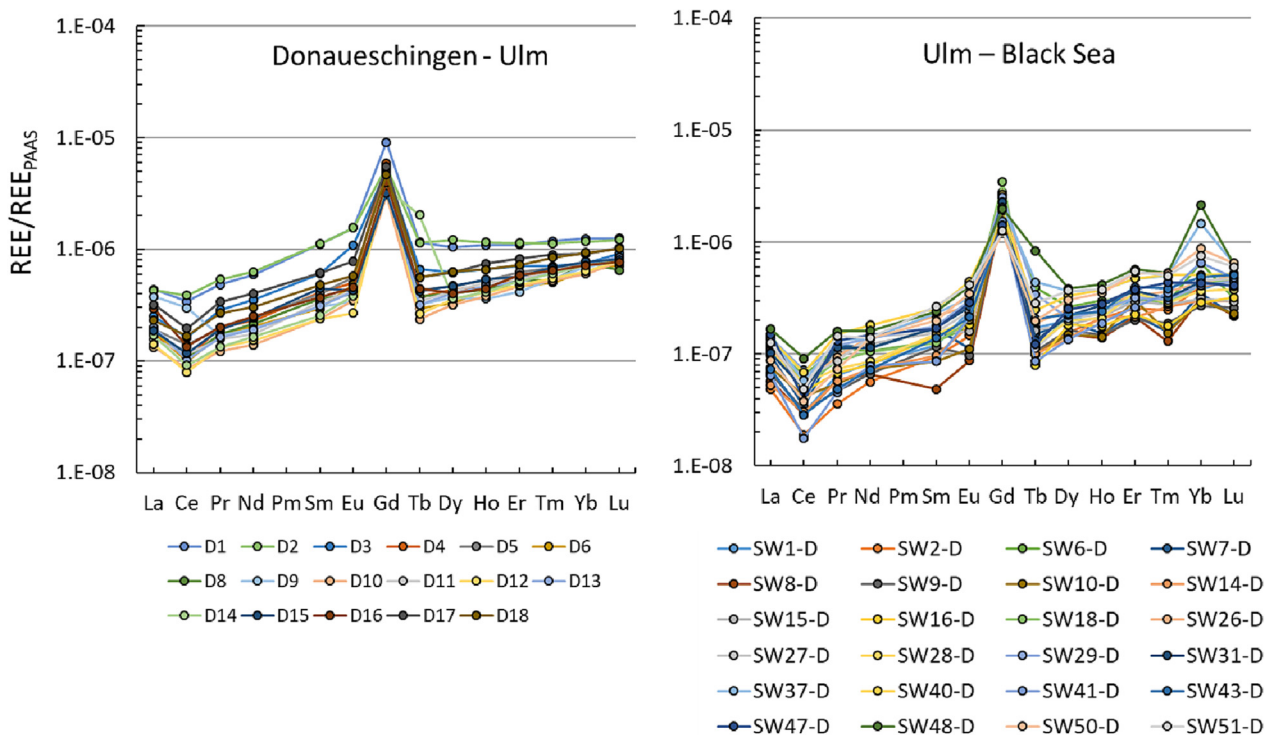
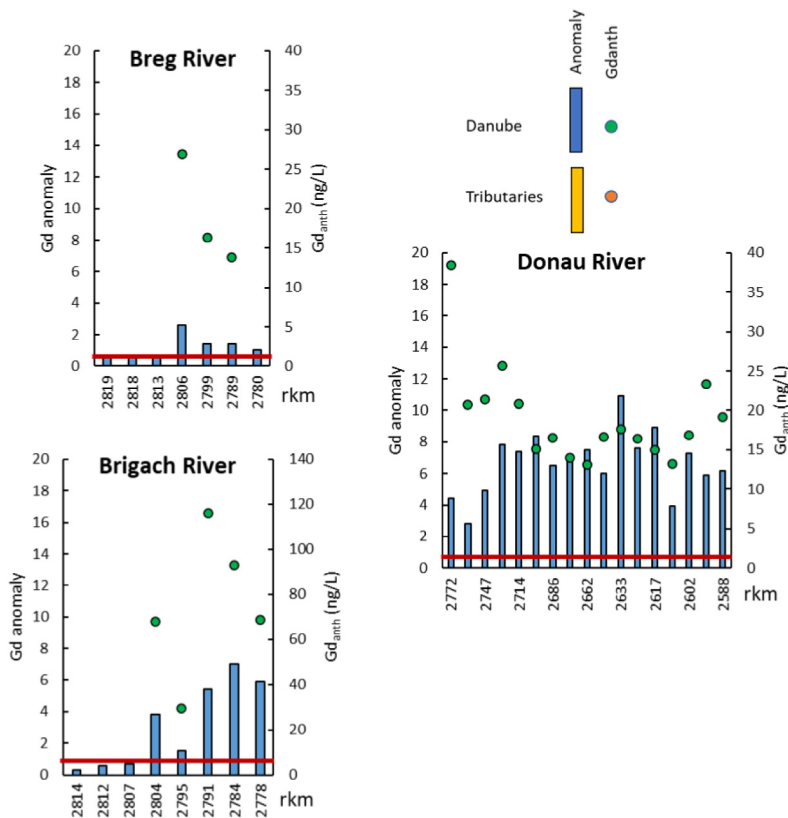


Fig. 8. REE patterns, normalized with respect to PAAS, along the Danube River, downstream Donaueschingen.

a)



b)

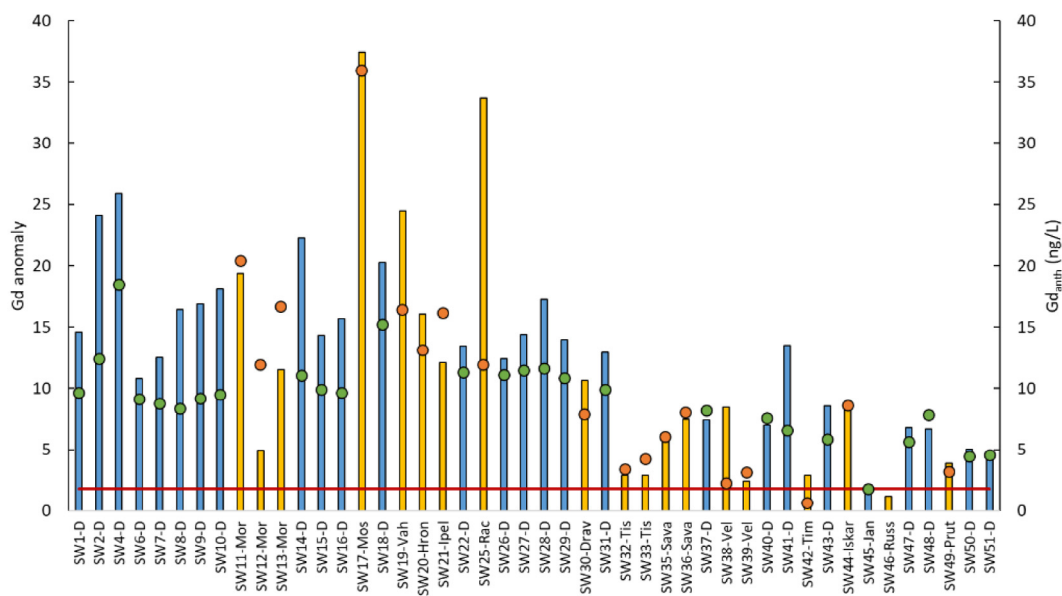


Fig. 9. Gd anomaly and Gd<sub>anth</sub> concentration downstream from the sources to Ulm (a) and from Ulm to the delta (b) for the Danube River and its tributaries. The red line corresponds to the limit value of Gd/Gd\* (1.5) proposed by Bau et al. (2006).

and in its tributaries: from sample SW-D1 (Boefinger Halede) to sample SW-D31 (Ilok), with a Gd/Gd\* globally above 10 and from sample SW-32 (Tisza) to sample SW-51D (Vilkova), with a Gd/Gd\* globally below 10. Gd anomaly and Gd<sub>anth</sub> concentration in these two groups can be related to the number of MRI units and MRI exams in each crossed country (Fig. 10). It is interesting to note that the average Gd<sub>anth</sub> concentration between SW1 and SW31 (11 ng/L ± 2.5 n/L) is quite stable and does not closely follow the fluctuations in Gd anomalies (Fig. 9).

Fig. 10 was built using data on the location and capacity of wastewater treatments plants along the Danube River and its main tributaries (expressed in persons-equivalent served). The data were collected from the Urban Waste Water Treatment Directive dissemination platform for EU countries (2016 data) and ICPDR data for non-EU countries. A total of 1546 wastewater treatment plants was considered. For each tributary, the contribution in terms of population to the Danube River watershed was also taken into account, as well as the eventual sharing of the tributary watershed between different countries.

In the first group (Austria, Czech Republic, Slovakia, Hungary, Croatia), the number of MRI exams/year/inhabitants is between 4000 and 6000, while it exceeds 14,000 exams/year/inhabitants in Germany (Fig. S7). In the second group (Serbia, Bulgaria, Romania), MRI exams/year/inhabitants are below 2000 and data are missing for Moldavia and Ukraine. The low number of MRI exams in Bulgaria can explain why there is no Gd/Gd\* detected in sample JDS4-46. The tipping point, where Gd/Gd\* becomes lower than 10, is Ilok (Croatia) (i.e. SW31-D). We note that the sampling plan of JDS4 for the Danube Delta region included only one site in the Chilia arm. The possible impact of the large city of Tulcea on REE pattern in the Sulina and Sfantu Gheorghe arms of the Danube Delta would require further consideration.

The groundwater wells close to the Danube River are also affected by anthropogenic Gd (Fig. S8). Gd-containing contrasting agents are synthesized not to easily release ionic Gd<sup>3+</sup>, which is extremely toxic, inside the human body. This otherwise desirable property makes them particularly difficult to degrade during drinking water treatment production and explains the presence of Gd in tap water.

It can be expected that the situation will not improve in the near future (Lachaux et al., 2022). The risk associated with Gd might even increase with the application of advanced technologies designed to degrade urban micropollutants in wastewater treatments plants, with the ultimate goals to reduce aquatic ecosystems contamination on one hand and potentially reuse treated wastewater on another hand. The risk associated with the dissemination of free Gd<sup>3+</sup> cannot be ignored considering the possible degradation of Gd-based contrast agents (Oluwasola et al., 2022).

The annual flux of Gd<sub>anth</sub> to the Black Sea, based on a total discharge just upstream of the delta of 6500 m<sup>3</sup>/s, is estimated at 0.9 ton/year,

corresponding to 11 kg/year/million inhabitants. This is of the same order of magnitude as the flux discharged by the Garonne River in France (14 kg/year/million inhabitants) (Lerat-Hardy et al., 2019). The annual flux is comparable with the annual flux of other large watersheds, such as the Saint-Laurent Estuary and Gulf in Canada (0.9 ± 0.7 ton/year) (Dang et al., 2022) and the Pearl River (0.6 ± 0.6 ton/year for about 84 million inhabitants) (Ma and Wang, 2023).

Finally, an Ytterbium anomaly seems to appear at some sampling sites close to the delta, in particular in stations SW-D37 and SW-D48. This anomaly is also clear on two tributaries, the Sava River and the Velika Morava River. No information related to such an anomaly could be found in the literature. Ytterbium is not largely used: its main uses are related to the improvement of stainless-steel properties and the production of lasers. However, sedimentary phosphate deposits (Emsbo et al., 2015) and their dumped residues from fertilizer production can contain ytterbium (Zirnea et al., 2013), which can be leached toward water bodies.

#### 4. Conclusions

At short distance from their sources the Brigach River and Breg River present REE patterns already influenced by the release in the aquatic environment of anthropogenic Gd. The Gd concentration in the Danube River is influenced by the development of MRI facilities and examinations. The slow decrease of the La/Lu ratio between Ulm and the Black Sea indicates an increasing anthropogenic influence as the Danube River flows downstream. As this survey was the first one to analyze REEs in the Danube River basin, future work will focus on consolidating the data with an increase of the number of sampling points in the Middle and Lower sections of the Danube as well as along the largest tributaries. Analysis of sediments could also bring information on the distribution of REE in the watershed. Although the monitoring of REE and the understanding of their origin and fate in large and complex watersheds are not easy tasks, they should be pursued, taking the example of the logistics developed during JDS4.

#### CRedit authorship contribution statement

**PL:** Investigation, Methodology, Data curation, Writing original draft. **SP:** Analysis. **DALV:** Formal analysis, Writing review and editing, Supervision. **MNP:** Investigation, Conceptualization, Supervision, Project administration, Funding acquisition, Writing review and editing.

#### Data availability

Data will be made available on request.

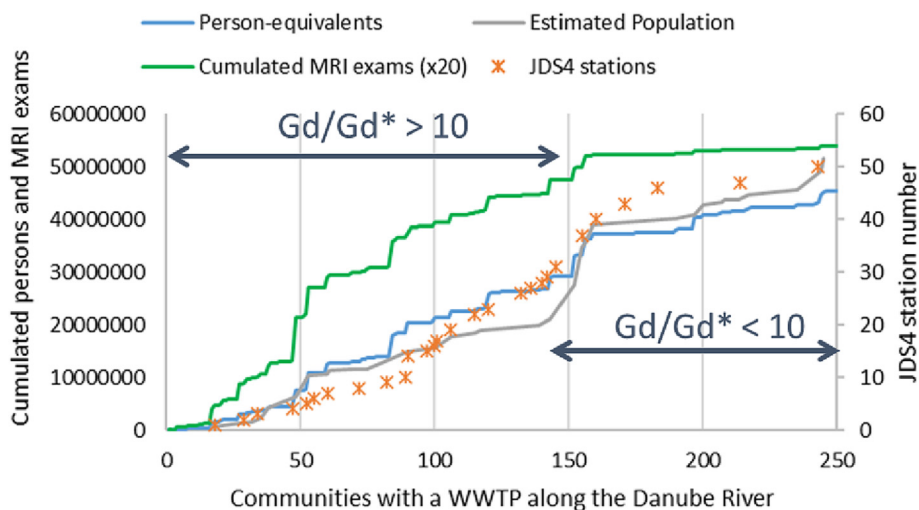


Fig. 10. Gd anomaly in the Danube River watershed in as a function of the population and the number of MRI exams.

## Declaration of competing interest

The authors declare that they have no known competing financial interests or personal relationships that could have appeared to influence the work reported in this paper.

## Acknowledgments

The authors acknowledge the financial support from the National Agency for Research – France (ANR) through the project ANR-16-CE34-0012-001 and of the LIFE Program (ENV.780956). The support of ICPDR and Norman network is greatly acknowledged.

## Appendix A. Supplementary data

Supplementary data to this article can be found online at <https://doi.org/10.1016/j.scitotenv.2023.164368>.

## References

- Amyot, M., Clayden, M.G., MacMillan, G.A., Perron, T., Arscott-Gauvin, A., 2017. Fate and trophic transfer of rare earth elements in temperate lake food webs. *Environ. Sci. Technol.* 51, 6009–6017. <https://doi.org/10.1021/acs.est.7b00739>.
- Assaad, A., Pontvianne, S., Corriou, J.P., Pons, M.N., 2015. Spectrophotometric characterization of dissolved organic matter in a rural watershed: the Madon River (N-E France). *EMAS* 187, 188. <https://doi.org/10.1007/s10661-015-4422-9>.
- Baker, A., 2002. Fluorescence properties of some farm wastes: implications for water quality monitoring. *Wat. Res.* 36, 189–195. [https://doi.org/10.1016/S0043-1354\(01\)00210-X](https://doi.org/10.1016/S0043-1354(01)00210-X).
- Bau, M., Dulski, P., 1996. Anthropogenic origin of positive gadolinium anomalies in rivers waters. *Earth Planet. Sci. Lett.* 143, 245–255. [https://doi.org/10.1016/0012-821X\(96\)00127-6](https://doi.org/10.1016/0012-821X(96)00127-6).
- Bau, M., Knappe, A., Dulski, P., 2006. Anthropogenic gadolinium as a micropollutant in river waters in Pennsylvania and in Lake Erie, northeastern United States. *Chem. Erde* 66, 143–152. <https://doi.org/10.1016/j.chemer.2006.01.002>.
- Becci, A., Boelchini, F., Amato, A., 2021. Sustainable strategies for the exploitation of end-of-life permanent magnets. *Processes* 9, 857. <https://doi.org/10.3390/pr9050857>.
- Boester, U., Rüde, T.R., 2020. Utilize gadolinium as environmental tracer for surface water-groundwater interaction in karst. *J. Contam. Hydrol.* 235, 103710. <https://doi.org/10.1016/j.jconhyd.2020.103710>.
- Chazot, A., Barrat, J.A., Jomaah, R., Ognard, J., Ben Salem, D., Gaha, M., 2020. Brain MRIs makeup the bulk of the gadolinium footprint in medical imaging. *J. Neuroradiol.* 47, 259–265. <https://doi.org/10.1016/j.neurad.2020.03.004>.
- Chen, Y., Huang, R., Guan, Y., Zhuang, T., Wang, Y., Tan, T., Wang, J., Zhou, R., Wang, B., Xu, J., Zhang, X., Zhou, K., Sun, R., Chen, M., 2021. The profiling of elements and pesticides in surface water in Nanjing, China with global comparisons. *Sci. Total Environ.* 774, 145749. <https://doi.org/10.1016/j.scitotenv.2021.145749>.
- Coble, P.G., 1996. Characterization of marine and terrestrial DOM in seawater using excitation-emission spectroscopy. *Mar. Chem.* 51, 325–346. [https://doi.org/10.1016/0304-4203\(95\)00662-3](https://doi.org/10.1016/0304-4203(95)00662-3).
- Dale, J.G., Cox, S.S., Vance, M.E., Marr, L.C., Hochella Jr., M.F., 2017. Transformation of cerium oxide nanoparticles from a diesel fuel additive during combustion in a diesel engine. *Environ. Sci. Technol.* 51, 1973–1980. <https://doi.org/10.1021/acs.est.6b03173>.
- Dang, D.H., Wang, W., Silma, A., Chatzis, A., Mucci, A., 2022. The contrasting estuarine geochemistry of rare earth elements between ice-covered and ice-free conditions. *Geochim. Cosmochim. Acta* 317, 488–506. <https://doi.org/10.1016/j.gca.2021.10.025>.
- Elderfield, H., Upstill-Goddard, R., Sholkovitz, E.R., 1990. The rare earth elements in rivers, estuaries, and coastal seas and their significance to the composition of ocean waters. *Geochim. Cosmochim. Acta* 54, 971–991. [https://doi.org/10.1016/0016-7037\(90\)90432-K](https://doi.org/10.1016/0016-7037(90)90432-K).
- Emsbo, P., McLaughlin, P.I., Breit, G.N., du Bray, E.A., Koenig, A.E., 2015. Rare earth elements in sedimentary phosphate deposits: solution to the global REE crisis? *Gondwana Res.* 27, 776–785. <https://doi.org/10.1016/j.jgr.2014.10.008>.
- Fraum, T.J., Ludwig, D.R., Bashir, M.R., Fowler, K.J., 2017. Gadolinium-based contrast agents: a comprehensive risk assessment. *J. Magn. Reson. Imaging* 46 (2), 338–353. <https://doi.org/10.1002/jmri.25625>.
- Han, R., Wang, Z., Shen, Y., Wu, Q., Liu, X., Cao, C., Gao, S., Zhang, J., 2021. Anthropogenic Gd in urban river water: a case study in Guiyang, SW China. *Elem. Sci. Anth.* 9, 1. <https://doi.org/10.1525/elementa.2020.00147>.
- Hissler, C., Hostache, R., Iffly, J.F., Pfister, L., Stille, P., 2015. Anthropogenic rare earth element fluxes into floodplains: coupling between geochemical monitoring and hydrodynamic sediment transport modelling. *C. R. Geosci.* 347, 294–303. <https://doi.org/10.1016/j.crte.2015.01.003>.
- Hobohm, J., Kuchta, K., Krüger, O., van Wasen, S., Adam, C., 2016. Optimized elemental analysis of fluorescence lamp shredder waste. *Talanta* 147, 615–620. <https://doi.org/10.1016/j.talanta.2015.09.068>.
- Hu, Z., Richet, H., Sparovek, G., Schnug, E., 2004. Physiological and biochemical effects of rare earth elements on plants and their agricultural significance: a review. *J. Plant Nutr.* 271, 183–220. <https://doi.org/10.1081/PLN-120027555>.
- JDS4, 2021. In: Liška, I., Wagner, F., Sengl, M., Deutsch, K., Slobodník, J., Paunović, M. (Eds.), *Scientific Report: A Shared Analysis of the Danube River Basin*. ISBN: 978-3-200-07450-7, Vienna, Austria. <http://www.danubsurvey.org/jds4/publications/scientific-report>.
- Joint Danube Survey 3, 2015. In: Liška, I., Wagner, F., Sengl, M., Deutsch, K., Slobodník, J. (Eds.), *A Comprehensive Analysis of Danube Water Quality*. ISBN: 978-3-200-03795-3, Vienna, Austria. [http://www.danubsurvey.org/jds3/jds3-files/nodes/documents/jds3\\_final\\_scientific\\_report\\_1.pdf](http://www.danubsurvey.org/jds3/jds3-files/nodes/documents/jds3_final_scientific_report_1.pdf). ISBN: 978-3-200-03795-3, Vienna, Austria.
- Kaegi, R., Gogos, A., Voegelin, A., Hug, S.J., Winkel, L.H.E., Buser, A.M., Berg, M., 2021. Quantification of individual rare earth elements from industrial sources in sewage sludge. *Water Res.* X 11, 1000092. <https://doi.org/10.1016/j.wroa.2021.100092>.
- Khan, A.M., Yusoff, I., Abu Bakar, N.K., Abu Bakar, A.F., Alias, Y., 2016. Assessing anthropogenic levels, speciation, and potential mobility of rare earth elements (REEs) in ex-tin mining area. *Environ. Sci. Pollut. Res.* 23, 25039–25055. <https://doi.org/10.1007/s11356-016-7641-x>.
- Kondor, A.C., Jakab, G., Vancsik, A., Filep, T., Szeberényi, J., Szabó, L., Maász, G., Ferincz, A., Dobosy, P., Szalai, Z., 2020. Occurrence of pharmaceuticals in the Danube and drinking water wells: efficiency of riverbank filtration. *Environ. Pollut.* 265, 114893. <https://doi.org/10.1016/j.envpol.2020.114893>.
- Kulaksız, S., Bau, M., 2011a. Rare earth elements in the Rhine River, Germany: first case of anthropogenic lanthanum as a dissolved microcontaminant in the hydrosphere. *Environ. Int.* 37, 973–979. <https://doi.org/10.1016/j.envint.2011.02.018>.
- Kulaksız, S., Bau, M., 2011b. Anthropogenic gadolinium as a microcontaminant in tap water used as drinking water in urban areas and megacities. *Appl. Geochem.* 26, 1877–1885. <https://doi.org/10.1016/j.apgeochem.2011.06.011>.
- Kulaksız, S., Bau, M., 2013. Anthropogenic dissolved and colloid/nanoparticle-bound samarium, lanthanum and gadolinium in the Rhine River and the impending destruction of the natural rare earth element distribution in rivers. *Earth Planet Sci. Lett.* 362, 43–50. <https://doi.org/10.1016/j.epsl.2012.11.033>.
- Lachaux, N., Cossu-Leguille, C., Poirier, L., Gross, E.M., Giamberini, L., 2022. Integrated environmental risk assessment of rare earth elements mixture on aquatic ecosystems. *Front. Environ. Sci.* 10, 974191. <https://doi.org/10.3389/fenvs.2022.974191>.
- Lavezzo, B., Kinoshita, A., Figueiredo, A.M.G., Pinheiro, M.M.F., Santa, W., 2020. Detection of rare-earth elements using fiddler crabs *Leptuca leptodactyla* (Crustacea: Ocypodidae) as bioindicators in mangroves on the coast of São Paulo, Brazil. *Sci. Total Environ.* 738, 139787. <https://doi.org/10.1016/j.scitotenv.2020.139787>.
- Le Goff, S., Barrat, J.A., Chauvaud, L., Paulet, Y.M., Gueguen, B., Ben Salem, D., 2019. Compound-specific recording of gadolinium pollution in coastal waters by great scallops. *Sci. Rep.* 9, 8015. <https://doi.org/10.1038/s41598-019-44539-y>.
- Lerat-Hardy, A., Coynel, A., Dutruch, L., Pereto, C., Bossy, C., Gil-Diaz, T., Capdeville, M.J., Blanc, G., Schäfer, J., 2019. Rare earth element fluxes over 15 years into a major European Estuary (Garonne-Gironde, SW France): hospital effluents as a source of increasing gadolinium anomalies. *Sci. Total Environ.* 656, 400–420. <https://doi.org/10.1016/j.scitotenv.2018.11.343>.
- Liu, W.S., Guo, M.N., Liu, C., Yuan, M., Chen, X.T., Huot, H., Zhao, C.M., Tang, Y.T., Morel, J.L., Qiu, R.L., 2019. Water, sediment and agricultural soil contamination from an ion adsorption rare earth mining area. *Chemosphere* 216, 75–83. <https://doi.org/10.1016/j.chemosphere.2018.10.109>.
- Lortholary, M., Zalouk-Vergnoux, A., Couderc, M., Kamari, A., François, Y., Herrenknecht, C., Poirier, L., 2020. Rare earth element bioaccumulation in the yellow and silver European eel (*Anguilla anguilla*): a case study in the Loire estuary (France). *Sci. Total Environ.* 719, 134938. <https://doi.org/10.1016/j.scitotenv.2019.134938>.
- Louis, P., Messaoudene, A., Jrad, H., Adboul-Hamid, B.A., Vignati, D.A.L., Pons, M.N., 2020. Understanding rare earth elements concentrations, anomalies and fluxes at the river basin scale: the Moselle River (France) as a case study. *Sci. Total Environ.* 742, 140619. <https://doi.org/10.1016/j.scitotenv.2020.140619>.
- Ma, L., Wang, W.X., 2023. Dissolved rare earth elements in the Pearl River Delta: using Gd as a tracer of anthropogenic activity from river towards the sea. *Sci. Total Environ.* 856, 159241. <https://doi.org/10.1016/j.scitotenv.2022.159241>.
- Martin, L.A., Vignati, D.A.L., Hissler, C., 2021. Contrasting distribution of REE and yttrium among particulate, colloidal and dissolved fractions during low and high flows in peri-urban and agricultural river systems. *Sci. Total Environ.* 790, 148207. <https://doi.org/10.1016/j.scitotenv.2021.148207>.
- McLennan, S.M., 1989. Rare earth elements in sedimentary rocks; influence of provenance and sedimentary processes. *Rev. Mineral. Geochem.* 21, 169–200.
- Merschel, G., Bau, M., 2015. Rare earth elements in the aragonitic shell of freshwater mussel *Corbicula fluminea* and the bioavailability of anthropogenic lanthanum, samarium and gadolinium in river water. *Sci. Total Environ.* 533, 91–101. <https://doi.org/10.1016/j.scitotenv.2015.06.042>.
- Mouchi, V., Godbillot, C., Forest, V., Ulianov, A., Lartaud, F., de Raféls, M., Emmanuel, L., Verrecchia, E.P., 2020. Rare earth elements in oyster shells: provenance discrimination and potential vital effects. *Biogeosciences* 17, 2205–2217. <https://doi.org/10.5194/bg-17-2205-2020>.
- Oluwasola, I.E., Ahmad, A.L., Shoparwe, N.F., Ismail, S., 2022. Gadolinium based contrast agents (GBCAs): uniqueness, aquatic toxicity concerns, and prospective remediation. *J. Contam. Hydrol.* 250, 104057. <https://doi.org/10.1016/j.jconhyd.2022.104057>.
- Pereto, C., Coynel, A., Lerat-Hardy, A., Gourves, P.Y., Schäfer, J., Baudrimont, M., 2020. *Corbicula fluminea*: a sentinel species for urban rare earth element origin. *Sci. Total Environ.* 732, 138552. <https://doi.org/10.1016/j.scitotenv.2020.138552>.
- Porvali, A., Agarwal, V., Lundström, M., 2020. REE(III) recovery from spent NiMH batteries as REE double sulfates and their simultaneous hydrolysis and wet-oxidation. *Waste Manag.* 107, 66–73. <https://doi.org/10.1016/j.wasman.2020.03.042>.
- Rabiet, M., Brissaud, F., Seidel, J.L., Pistre, S., Elbaz-Poulichet, F., 2009. Positive gadolinium anomalies in wastewater treatment plant effluents and aquatic environment in the Hérault watershed (South France). *Chemosphere* 75, 1057–1064. <https://doi.org/10.1016/j.chemosphere.2009.01.036>.

- Rétif, J., Zalouk-Vergnoux, A., Briant, N., Poirier, L., 2023. From geochemistry to ecotoxicology of rare earth elements in aquatic environments: diversity and uses of normalization reference materials and anomaly calculation methods. *Sci. Total Environ.* 856, 158890. <https://doi.org/10.1016/j.scitotenv.2022.158890>.
- Santos, A.C.S.S., Souza, L.A., Araujo, T.G., de Rezende, C.E., Hatje, V., 2023. Fate and trophic transfer of rare earth elements in a tropical estuarine food web. *Environ. Sci. Technol.* 57, 2004–2014. <https://doi.org/10.1021/acs.est.2c07726>.
- Seto, M., Akagi, T., 2008. Chemical condition for the appearance of a negative Ce anomaly in stream waters and groundwaters. *Geochem. J.* 42, 371–380. <https://doi.org/10.2343/geochemj.42.371>.
- Shajib, M.T.I., Hansen, H.C.B., Liang, T., Holm, P.E., 2020. Rare earth elements in surface specific urban runoff in Northern Beijing. *Sci. Total Environ.* 717, 136969. <https://doi.org/10.1016/j.scitotenv.2020.136969>.
- Souza, L.A., Pedreira, R.M.A., Miró, M., Hatje, V., 2021. Evidence of high bioaccessibility of gadolinium-contrast agents in natural waters after human oral uptake. *Sci. Total Environ.* 793, 148506. <https://doi.org/10.1016/j.scitotenv.2021.148506>.
- Tepe, N., Romeo, M., Bau, M., 2014. High-technology metals as emerging contaminants: strong increase of anthropogenic gadolinium levels in tap water of Berlin, Germany, from 2009 to 2012. *Appl. Geochem.* 45, 191–197. <https://doi.org/10.1016/j.apgeochem.2014.04.006>.
- Thomsen, H.S., 2017. Are the increasing amounts of gadolinium in surface and tap water dangerous? *Acta Radiol.* 8 (3), 259–263. <https://doi.org/10.1177/0284185116666419>.
- Turra, C., 2018. Sustainability of rare earth elements chain: from production to food – a review. *Int. J. Environ. Health R.* 2 (1), 23–42. <https://doi.org/10.1080/09603123.2017.1415307>.
- Valdés-Vilchis, S., Sánchez-Beristain, J.P., Bernal, C., Juárez, E.A., 2021. Rare Earth Elements and Yttrium (REE + Y) patterns in recent *Anadara brasiliana* shells from Playa Norte, Barra de Cazon (Veracruz, Mexico): evidence of anthropogenic contamination linked to river output? *J. S. Am. Earth Sci.* 110, 103368. <https://doi.org/10.1016/j.jsames.2021.103368>.
- Veiga, M., Mattiazzi, P., de Gois, J.S., Nascimento, P.C., Borges, D.L.G., Bohrer, D., 2020. Presence of other rare earth metals in gadolinium-based contrast agents. *Talanta* 216, 120940. <https://doi.org/10.1016/j.talanta.2020.120940>.
- Yang, Y., Walton, A., Sheridan, R., Güth, K., Gauß, R., Gutfleisch, O., Buchert, M., Steenari, B.-M., Van Gerven, T., Jones, P.T., Binnemans, K., 2017. REE recovery from end-of-life NdFeB permanent magnet scrap: a critical review. *J. Sustain. Metall.* 3, 122–149. <https://doi.org/10.1007/s40831-016-0090-4>.
- Yeghicheyan, D., Aubert, D., Bouhnik-Le Coz, M., Chmeleff, J., Delpoux, S., Djouaev, I., Granier, G., Lacan, F., Piro, J., Rousseau, T., Cloquet, C., Marquet, A., Menniti, C., Pradoux, C., Freydier, R., Vieira da Silva-Filho, E., Suchorski, K., 2019. A new interlaboratory characterisation of silicon, rare earth elements and twenty-two other trace element concentrations in the natural river water certified reference material SLRS-6 (NRC - CNRC). *Geostand. Geoanal. Res.* 43, 475–496. <https://doi.org/10.1111/ggr.12268>.
- Zhang, C., Wang, L., Zhang, S., 1998. Geochemistry of rare earth elements in the mainstream of the Yangtze River, China. *Appl. Geochem.* 13, 451–462. [https://doi.org/10.1016/S0883-2927\(97\)00079-6](https://doi.org/10.1016/S0883-2927(97)00079-6).
- Zirnea, S., Lazar, I., Saha Foudjoa, B.U., Vasilache, T., Lazar, G., 2013. Cluster analysis based of geochemical properties of phosphogypsum dump located near Bacau City in Romania. *APCBEE Proc.* 5, 317–322. <https://doi.org/10.1016/j.apcbee.2013.05.05>.